

RESEARCH ARTICLE

FTIR autecological analysis of bottom-ice diatom taxa across a tidal strait in the Canadian Arctic

Nicole M. Pogorzelec¹, Kathleen M. Gough^{2,*}, Sun-Yong Ha³, Karley Campbell^{1,4}, Brent Else⁵, Kwanwoo Kim⁶, Sang Heon Lee⁶, and C. J. Mundy^{1,*}

A recent study demonstrated that an Arctic tidal strait, where a shoaled and constricted waterway increases tidally driven sub-ice currents and turbulence, represents a “hotspot” for ice algal production due to a hypothesized enhanced ocean-ice nutrient supply. Based on these findings, we sampled the bottom-ice algal community across the same tidal strait between the Finlayson Islands within Dease Strait, Nunavut, Canada, in spring 2017. Our objective was to examine cellular responses of sea-ice diatoms to two expected nutrient supply gradients in their natural environment: (1) a horizontal gradient across the tidal strait and (2) a vertical gradient in the bottom-ice matrix. Two diatom taxa, *Nitzschia frigida* and *Attheya* spp. in bottom-ice sections (0–2, 2–5, and 5–10 cm) under thin snow cover (<5 cm), were selected for Fourier Transform Infrared (FTIR) spectrochemical analysis for lipid and protein content. Results from the FTIR technique strongly supported the existence of a horizontal nutrient gradient across the tidal strait of the Finlayson Islands, while estimates of particulate organic carbon and chlorophyll *a* concentrations were difficult to interpret. The larger *N. frigida* cells appeared to be more sensitive to the suspected horizontal nutrient gradient, significantly increasing in lipid content relative to protein beyond the tidal strait. In contrast, the epiphytic diatoms, *Attheya* spp., were more sensitive to the vertical gradient: above 2 cm in the bottom-ice matrix, the non-motile cells appeared to be trapped with a depleted nutrient inventory and evidence of a post-bloom state. Application of the FTIR technique to estimate biomolecular composition of algal cells provided new insights on the response of the bottom-ice algal community to the examined spatial gradients that could not be obtained from conventional bulk measurements alone. Future studies of sea ice and associated environments are thus encouraged to employ this technique.

Keywords: FTIR spectroscopy, Biomolecular composition, Ice algae, Nutrient concentrations, Diatom, Arctic

Introduction

Sea-ice algae are important primary producers during early spring, synthesizing high-energy essential fatty acids that sustain the Arctic marine food web (Smith et al., 1987; Mock and Gradinger, 2000; Mock and Thomas, 2005; Leu et al., 2010; Søreide et al., 2010). The majority of Arctic sea-ice algal communities inhabit the bottommost 0–10 cm of sea ice (Horner et al., 1992; Arrigo, 2014; Leu et al., 2015), with diatoms being the dominant taxa during the spring bloom (Róžańska et al., 2009; Poulin et al., 2011; van

Leeuwe et al., 2018). The bloom of diatoms in sea ice begins under low-light and nutrient-replete conditions during late winter to early spring (Leu et al., 2015). However, the rise in average global temperatures has resulted in a decline in sea-ice extent and thickness, caused by later freeze-up and longer melt period (Comiso et al., 2008; Markus et al., 2009; Stroeve et al., 2012). These rapid changes affect the phenology and contribution of ice algae to total primary production in the Arctic (Tedesco et al., 2019), with the potential of a cascading effect on the marine food web (Michel et al., 2006; Søreide et al., 2010).

Bottom-ice photosynthetically active radiation (PAR) is limited by sea-ice thickness and, more importantly, by the high albedo and strong attenuation properties of the overlying snow cover (Perovich et al., 1998; Perovich, 2018). As a result, spring ice algal biomass often has a significant negative relationship with snow depth (Campbell et al., 2015). However, during their spring bloom, ice algae experience a transition from initial light limitation to nutrient limitation, as light increases and algal growth demand exceeds available nutrients in the sea-ice matrix (Cota et al., 1987; Campbell et al., 2016).

¹Centre for Earth Observation Science (CEOS), Department of Environment and Geography, University of Manitoba, Winnipeg, MB, Canada

²Department of Chemistry, University of Manitoba, Winnipeg, MB, Canada

³Korea Polar Research Institute (KOPRI), Incheon, South Korea

⁴University of Tromsø, Tromsø, Norway

⁵University of Calgary, Calgary, AB, Canada

⁶Pusan National University, Busan, South Korea

* Corresponding authors:

Emails: cj.mundy@umanitoba.ca; kathleen.gough@umanitoba.ca

The main nutrient supply to the bottom-ice algal community is from the underlying water column across the ocean-ice boundary layer (Gosselin et al., 1985; Cota et al., 1987; Dalman et al., 2019). A strong temperature gradient in the ice bottom from the warm ocean to colder atmosphere in winter and spring reduces brine volume space, thereby reducing convection of nutrient-carrying brine higher into the ice matrix (Vancoppenolle et al., 2013). Therefore, nutrient supply to the ice algal community is expected to decrease with vertical distance above the ocean-ice interface. Comparing locations along a horizontal transect, Dalman et al. (2019) concluded that tidal straits (shoaled and constricted waterways dominated by tidal current flow) represent localized hotspots of ice algal production. This conclusion was derived from observations of increased tidally driven currents and mixing, reduced stratification, and greater ice algal biomass towards the centre of a tidal strait. Therefore, greater currents towards the centre of a tidal strait are expected to enhance ocean-ice nutrient flux to the bottom-ice algae.

Arctic sea-ice diatoms can store photosynthetically allocated carbon as either lipid, protein, polysaccharides, or low molecular weight metabolites when subjected to environmental stress (Smith et al., 1987; Smith et al., 1997). Here we focus on lipid and protein content of individual diatom cells. An increase in the intensity of PAR results in an increase in cellular photosynthetic rate and lipid production, while a decrease in nutrient (i.e., nitrate) availability can result in increased lipid storage and a decreased protein production (Mock and Kroon, 2002a; 2002b; Pogorzelec et al., 2017).

Fourier transform infrared (FTIR) spectrochemical analysis is a long-established method for quantitative and qualitative identification and analysis of the chemical composition of materials (Hollas, 2004; Griffiths and de Haseth, 2007). Infrared light has the appropriate energy for excitation of internal molecular motions (vibrations) that are characteristic for different functional groups (Herzberg, 1945). Several studies have demonstrated that FTIR spectroscopy and imaging are efficient methods for measuring the relative abundance of cellular lipid (CH_2+CH_3) and protein (Amide I) content in diatoms, enabling an analysis of their response to light and nutrient stress (Giordano et al., 2001; Stehfest et al., 2005; Sackett et al., 2013; Findlay et al., 2015; Sackett et al., 2016; Pogorzelec et al., 2017). In this study, we used FTIR spectrochemical imaging to assess the biomolecular composition of individual diatom cells in response to the two aforementioned expected nutrient supply gradients: (1) a horizontal gradient across a tidal strait and (2) a vertical gradient in the bottom-ice matrix, upwards through 0–2, 2–5, and 5–10 cm sections. Single cell FTIR analysis supported the exciting opportunity to undertake this autecological research of the sea-ice community (Pogorzelec et al., 2017).

The Kitikmeot Sea in the western Canadian Arctic is a highly nitrogen-depleted system (Campbell et al.,

2017; Pogorzelec et al., 2017; Kim et al., 2020), creating a logical location to examine the impacts of nutrient gradients on a natural ice algal community (Dalman et al., 2019). We hypothesized that greater nutrient supply occurs in the bottommost ice sections and at the centre of the tidal strait, resulting in detectable increases in protein production and decreases in lipid storage. Samples were collected over a 2-week period in April and May during the 2017 Ice Covered Ecosystem-Cambridge Bay Process Study (ICE-CAMPS) campaign. Contrasting responses in biomolecular composition were observed for two diatom taxa, *Nitzschia frigida* (pennate) and *Attheya* spp. (centric), with implications for species succession in the system.

Methods

Field collection

Samples were collected from four sample sites on April 28, May 3, and May 9 during the 2017 ICE-CAMPS field campaign. The field sites were located on landfast sea ice within a tidal strait area between the Finlayson Islands, in the Kitikmeot Sea, Nunavut, Canada. Sample sites (**Figure 1**) were spaced along a transect from inside (sites 1 and 2) to outside (sites 3 and 4) the tidal strait, in order to access variation in under-ice currents and water-column mixing according to Dalman et al. (2019). At each site, four ice cores were collected under thin snow cover (<5 cm depth) using a 9-cm inner diameter Mark II Coring System (Kovacs Enterprises). After extraction, ice cores were kept shaded to minimize potential changes to the biomolecular composition of the ice algae (Leu et al., 2010; Stitt et al., 2012). The bottom 10-cm length of each core was segmented into sections of 0–2, 2–5, and 5–10 cm for diatom collection. An additional 10-cm bottom-ice core was collected and sectioned into 0–2, 2–5, and 5–10 cm ice sections for measurements of salinity (Thermo Scientific ORION STAR A212) and nutrient concentrations.

Core sections for particulate analysis were pooled in the dark within insulated containers for transport and melting. Filtered seawater (FSW; 0.2- μm membrane filter) was added to the containers at a 3:1 ratio (FSW:pooled ice cores) and left overnight to melt. The FSW was added to minimize osmotic stress on diatoms during sea-ice melt (Garrison and Buck, 1986; Rintala et al., 2014; Campbell et al., 2019). All particulate samples were corrected for FSW dilution.

Several environmental measurements were collected in conjunction with ice core collection, including snow depth, ice thickness, and spectral downwelling irradiance, albedo (upwelling:downwelling irradiance), and under-ice PAR transmittance. The spectral irradiance was measured with a hyperspectral radiometer (Satlantic HyperOCR) calibrated for air and water immersion. An articulating arm was used to position the sensor in the air above the snow to make measurements of downwelling and upwelling irradiance and then submersed through an auger hole to make downwelling transmitted irradiance measurements at the ocean-ice interface.

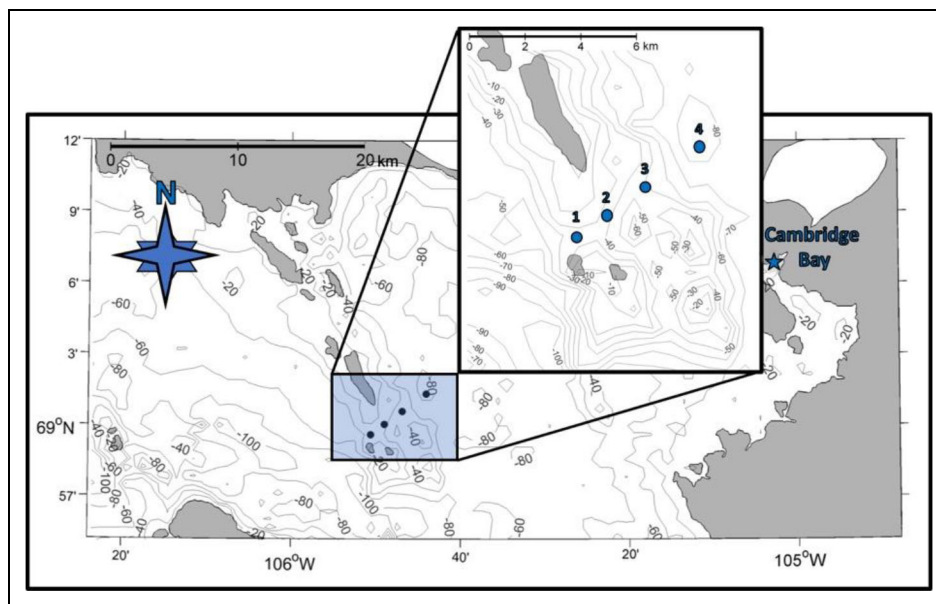


Figure 1. Map of sampling stations. Field site locations amid the Finlayson Islands, near Cambridge Bay, Nunavut, Canada. Sites 1 ($68^{\circ} 59.600'N$, $105^{\circ} 50.590'W$) through 4 ($69^{\circ} 01.320'N$, $105^{\circ} 44.040'W$), located along a 6-km transect, are denoted with blue dots; see magnified inset for greater detail. Bathymetry is in meters.

Nutrient analysis and bulk community sample collection

Ice core layers for dissolved nutrient concentration analysis were melted in the dark, without FSW, in a sterile Whirlpak bag. The ice melt was filtered through an acid-washed (10% HCl) Swinnex® filter holder with a GF/F filter, pre-combusted at $450^{\circ}C$ for 5 h, and stored in an acid-washed 15-mL falcon tube at $-20^{\circ}C$ until analysis at the Université du Québec à Rimouski. Concentrations of phosphate, nitrate+nitrite, and silicic acid were determined with a Seal Analytical Auto-Analyzer 3 as described in Grasshoff et al. (1999).

Taxonomy samples were prepared by combining 100 mL of FSW-diluted ice core melt and 4 mL of Lugol's Acid in a 125-mL amber glass bottle, which was stored at $4^{\circ}C$. Diatom taxonomic surveys and cell counts for target species, total pennate and centric diatoms, and other ice algal taxa (i.e., flagellate, dinoflagellate, and unknown) were accomplished with an inverted light microscope and Ütermohl type chamber, known as the Hydrobios method (Lund et al., 1958; Campbell et al., 2018).

Samples for measurement of particulate organic carbon (POC) were collected by filtration of 200 to 400 mL of FSW-diluted ice core melt in indirect light conditions onto a GF/F filter pre-combusted at $450^{\circ}C$ for 5 h, wrapped in a pre-combusted aluminum casing and stored at $-80^{\circ}C$. Samples were analyzed for POC concentration within 3 months using an Elemental Analyzer (Elementar Vario Micro Cube) as described in Cutter et al. (2014).

For chlorophyll *a* (Chl *a*) determination, 5 to 200 mL of FSW-diluted ice core melt was filtered onto a 25-mm GF/F filter and stored at $-80^{\circ}C$. The Chl *a* pigment was extracted from the filter by adding 10 mL of 90% acetone and storing the filter in the dark at $4^{\circ}C$ for 18 h before analysis. Chl *a* fluorescence was measured before and after acidification with 5% HCl (Parsons et al., 1984), using

a Turner Designs Trilogy Fluorometer and converted into Chl *a* concentration ($mg\ m^{-2}$) according to the equations described in Holm-Hansen et al. (1965).

FTIR data collection and analysis

All procedures were conducted in a darkened environment to prevent photo-oxidation of cellular fatty acids (Sattar et al., 1976; Stitt et al., 2012). Diatoms were collected by filtering 5 to 200 mL of FSW-diluted ice core melt onto a 5- μm pore size polycarbonate membrane filter (SterliTech Corp., USA). The filter was folded in half, wrapped in aluminum foil, and stored in a portable $-80^{\circ}C$ freezer, returned to the University of Manitoba, and moved to a $-80^{\circ}C$ freezer until analysis. For FTIR data collection, a frozen filter was placed on dry ice; a pie-shaped segment was cut out and the wrapped filter was returned to the $-80^{\circ}C$ freezer. Diatom cells were transferred onto a 25-mm diameter, 2-mm thick barium fluoride (BaF_2) substrate by pipetting a 4- μL ultra-pure (Milli-Q) water droplet on the substrate and placing a segment of the polycarbonate filter onto the droplet. The filter was agitated gently to release the diatoms which were then left to settle for approximately 1 min. Excess water was wicked away with a tissue (Kimwipe®). A compound light microscope equipped with a 650-nm red photo light filter to prevent photo-oxidation of lipids (Sattar et al., 1976; Stitt et al., 2012), was used to identify and select individual diatom cells for imaging. Substrates were placed in a desiccant chamber and in the dark with silica beads overnight prior to imaging.

Two dominant diatom taxa were targeted to obtain a range of cell sizes and to reflect main taxa in the winter-spring transition period (Poulin et al., 2011; Campbell et al., 2018; van Leeuwe et al., 2018). These included a pennate diatom, *Nitzschia frigida* (average cell size of $68 \times 8\ \mu m$; **Figure 2A**) and an epiphytic centric diatom,

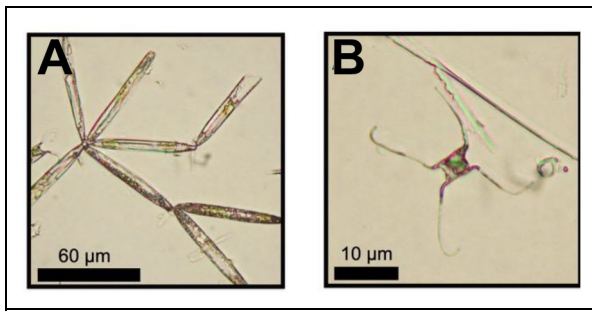


Figure 2. Light microscopic images of the targeted FTIR diatom taxa. Example images of the targeted diatom taxa: (A) an arborescent colony of *Nitzschia frigida* and (B) a single cell of *Attheya* spp.

Attheya spp. (average cell size of $9 \times 10 \mu\text{m}$, without setae; **Figure 2B**). Both are associated primarily with Arctic sea ice. The former has been described as a sentinel species for the Arctic spring ice algal bloom (Poulin et al., 2011). The latter dominates the centric diatom community in the study region, particularly in late spring as light increases and nutrients decrease (Campbell et al., 2017; Pogorzelec et al., 2017). Although identified as belonging to *A. septentrionalis* or *A. longicornis*, some cells were difficult to confirm, and thus the general classification of *Attheya* spp. was used.

Approximately 18 h after sample preparation, the infrared spectrochemical images of individual diatoms were obtained with an Agilent Cary 670 FTIR spectrometer coupled to a 620 IR imaging microscope operated in transmission mode (Pogorzelec et al., 2017). The IR microscope was equipped with a $15\times$ objective and condenser, numerical aperture 0.62, and a 64×64 focal plane array (FPA) detector that produced IR images with a field of view of approximately $70 \times 70 \mu\text{m}^2$ and a nominal spatial resolution of $1.1 \times 1.1 \mu\text{m}^2$ per pixel (Findlay et al., 2015; Pogorzelec et al., 2017). All spectral data were recorded at 8 cm^{-1} spectral resolution and a zero-fill factor of 2. A background image was recorded from a clear region of the substrate; 512 scans were co-added for the background image and 256 scans for each sample image, to ensure good signal to noise. Sample images were ratioed against the background to provide a full hyperspectral data cube; that is, a full infrared spectrum associated with each imaged pixel in the array, displayed as absorption intensity as a function of infrared photon energy, typically reported as inverse wavelength, or wavenumber, in units of cm^{-1} . The distribution of any biomarker could be displayed as a false colour image by integration of the band area, illustrating the strength of a chosen IR absorption band at each pixel within the array. Spectra and false-coloured images were processed initially for diatom biomolecular content in Resolutions ProTM (version 5.2.0, Agilent Technologies Inc.) as described elsewhere (Pogorzelec et al., 2017). The images were exported to MATLABTM for further processing to yield the composition of silicate, lipid and protein per diatom (Findlay et al., 2015; Pogorzelec et al., 2017). At

least 3 and up to 10 separate cells were used to calculate average (\pm standard error) composition values for each diatom taxon per sample.

Statistical analysis

Linear regression analyses were conducted to examine trends in variables across the tidal strait at horizontal transect sites 1–4. Regressions were performed only on data from the 0–2 cm ice sections, under the assumption that this layer was influenced most directly by ocean-ice fluxes (see below). Trends in the vertical ice sections were tested for differences using a two factor repeated measures ANOVA, while one-way ANOVA was used for cell count data, which was restricted to only a single sampling day (F-statistic; $\alpha = 0.05$). The repeated measures ANOVA was used to remove horizontal trends from the analysis. Prior to the ANOVA tests, data were tested for normality and equal variances using Shapiro-Wilk and Levene Median tests, respectively. All two-factor repeated measures ANOVA analyses passed these tests; however, the one-way ANOVA for cell counts failed the Shapiro-Wilk test; for that, a Kruskal-Wallis one-way ANOVA on ranks test (H-statistic) was used to test for significant differences between vertical ice sections. If the ANOVA was found to be significant, a Tukey's post hoc test was conducted to determine differences between ice section pairs.

Results

Physical and chemical environmental conditions

Snow depth decreased significantly from site 1 to site 4 (principally at site 4), while ice thickness increased significantly (**Figure 3A**). PAR albedo was consistent across sites, whereas percent PAR transmittance increased slightly from roughly 2% to 2.5% from sites 1 to 4, with snow depth lowest at site 4 (**Figure 3B**). Neither PAR albedo nor transmittance exhibited a trend across sites.

Within-site variability was high for salinity and nutrient concentrations in the bottommost 0–2 cm ice section, with some apparent outliers at site 1 for silicic acid, site 3 for phosphate, and site 4 for nitrate+nitrite (**Figure 4**). Across the horizontal transect, no significant relationships were observed between distance from the tidal strait (starting from site 1) and salinity and nutrient concentrations. In contrast, averaged nutrient concentrations across the four sites decreased upwards through the vertical layers. Bottom-ice salinity and nutrient concentrations were significantly greater in the bottom 0–2 cm ice section (Table S1). The mean values \pm standard deviation ($n = 12$) for phosphate, nitrate+nitrite, and silicic acid in the 0–2 cm layers were 4.9 ± 2.0 , 1.5 ± 0.9 , and $5.4 \pm 2.3 \text{ mmol L}^{-1}$; in the 5–10 cm layers, these values decreased to 0.2 ± 0.1 , 0.4 ± 0.2 and $0.9 \pm 0.5 \text{ mmol L}^{-1}$, respectively (**Figure 4B–D**; Table S1).

Ice algal community

Diatoms dominated the ice algal community; pennate and centric diatoms accounted for more than 80% of the population (**Figure 5A–C**). Relative abundance of other ice algal taxa (i.e., flagellate, dinoflagellate and unidentified taxa)

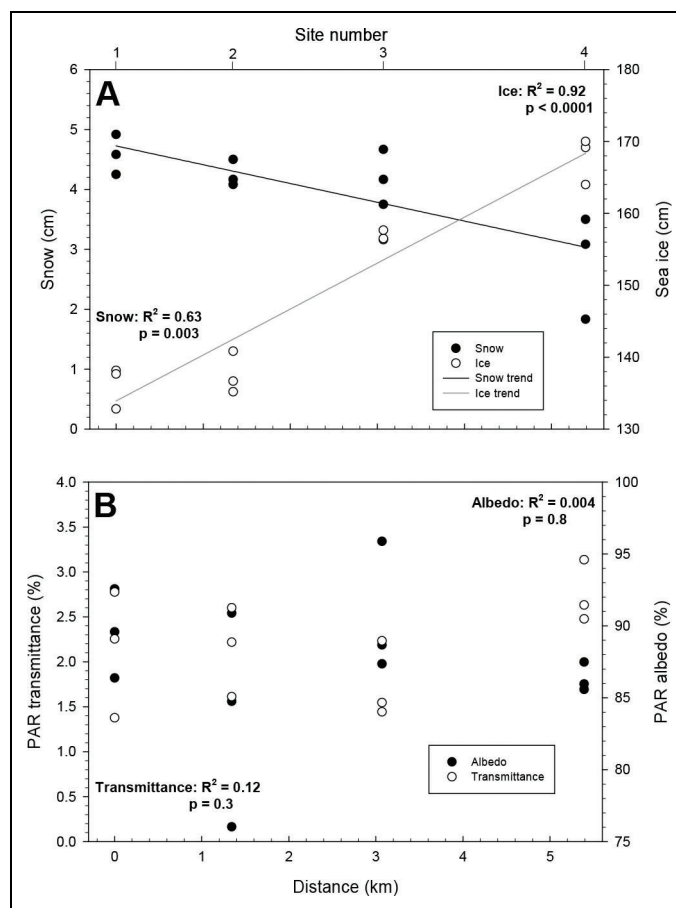


Figure 3. Pertinent physical conditions along the horizontal transect. (A) Snow depth ($y = 4.73 - 0.31x$), sea-ice thickness ($y = 133.9 + 6.4x$), and (B) percent PAR transmittance and albedo observed across sites 1–4 during the study. Lines in (A) show significant linear trends.

increased noticeably above the 0–2 cm ice section (Figure 5C), with the 2–5 and 5–10 cm sections having relatively equal proportions (Figure 5A and B).

Enumeration of intact diatom cells and empty frustules showed that the relative contribution of intact centric cells increased slightly upwards into the sea-ice matrix (from 13–20% to 18–27%), whereas that of pennates strongly decreased (65–85% to 16–29%; Figure 5D–F). Interestingly, the relative abundance of empty pennate frustules increased from the 0–2 cm section (6–18%; Figure 5F) towards the 5–10 cm ice section (43–61%; Figure 5D). Empty centric frustules, however, did not increase greatly in relative abundance (0.6–2% to 2–5%).

Of the two diatom species targeted for FTIR analysis (Figure 5G–I), *Attheya* spp. dominated the centric community (13% to 50%), especially above the 0–2 cm layer. In contrast, the relative abundance of *Nitzschia frigida* decreased noticeably from 12–25% in the 0–2 cm ice section to 0.2–4% in the 5–10 cm ice section. Both species decreased significantly in absolute abundance upwards into the ice matrix (Table 1). *Attheya* spp. exhibited epiphytic associations with pennate diatom cells (overwhelmingly associated with *N. frigida*) only in the 0–2 cm ice section, while cells were always observed as solitary in the 2–5 and 5–10 cm ice sections, where *N. frigida* was not abundant.

Particulate organic carbon was significantly greater in the 0–2 cm ice section (Table 1), with an average value of $500 \pm 170 \text{ mg m}^{-2}$ ($n = 12$) across all sites. In fact, all bulk measurements (i.e., POC, Chl *a* and POC:Chl *a*) were found to differ significantly in the vertical direction (two factor repeated measures ANOVA, $p < 0.01$) within most ice sections (Table 1). However, POC in the 0–2 cm ice section did not exhibit a significant dependence on location along the transect (Figure 6). In contrast, the Chl *a* concentration in the 0–2 cm ice section followed a significant decreasing trend away from the tidal strait (Figure 6B), dropping from $9.3 \pm 2.0 \text{ mg m}^{-2}$ at site 1 to $4.1 \pm 1.3 \text{ mg m}^{-2}$ at site 4. The POC:Chl *a* ratio (Figure 6C) tended to increase from site 1 to site 4; however, this apparent increase was not significant (Table 1).

Cellular biomass composition from FTIR

Diatom FTIR spectra and image analysis

FTIR spectra exhibited the typical profiles of diatoms (Findlay et al., 2015; Pogorzelec et al., 2017). All O-H and N-H stretch vibrations lie above 3000 cm^{-1} . Long acyl chain fats absorb very strongly in the energy region of $2800\text{--}3000 \text{ cm}^{-1}$ owing to excitation of CH-stretch vibrations. Unsaturated fatty acids containing the C=C-H functional group would also display a band around 3010 cm^{-1} . Where these lipids exist as fatty acid esters, a characteristic

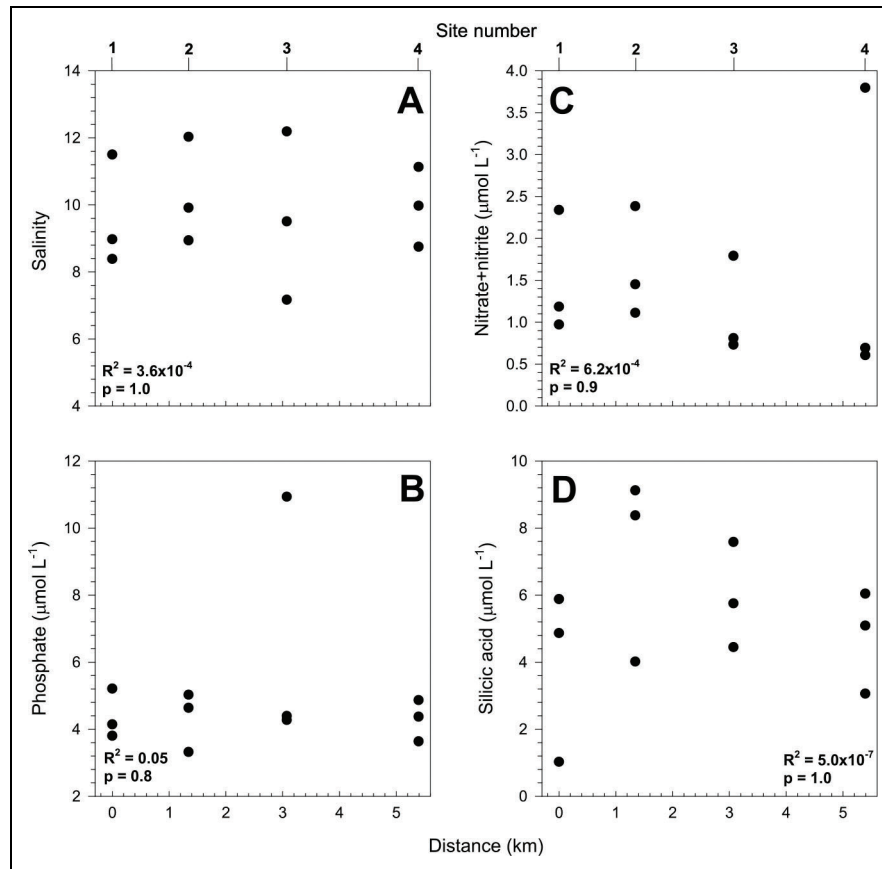


Figure 4. Bulk salinity and nutrient concentrations in bottommost sea ice along the horizontal transect. (A) Bulk salinity and concentrations of (B) phosphate, (C) nitrate+nitrite, and (D) silicic acid in the bottommost 0–2 cm sea-ice section from the 4 sample sites by distance along the sampling transect.

ester C=O stretch band occurs at approximately 1735 cm^{-1} . Proteins are identifiable from their characteristic amide vibrations, the amide I being primarily C=O stretch, while the amide II is described as a combination of C-N stretch and C-N-H angle bend. Other lipid bands are often discernible around 1380 and 1465 cm^{-1} , where the relative concentration of lipid fatty acid is high. While carbohydrates are usually identifiable by ring C-O-C absorption bands in the $950\text{--}1100\text{ cm}^{-1}$ region, the intense and broad absorption due to the Si-O bond, with a maximum around 1075 cm^{-1} , consistently obscured any carbohydrate signal. The Si-O band is ubiquitous, as the cells are observed in transmission mode, thus all light passes through the entire cell.

Spectra from a *Nitzschia frigida* diatom cell are shown in **Figure 7**, along with false-coloured FTIR images created to show the distribution of lipid, protein and silicate within diatoms. Spectra (**Figure 7A**) were selected from two visibly distinct locations (**Figure 7B**) to exemplify variation within a single diatom. While the spectral profiles are roughly similar, the total intensity of individual components is vastly different within the protein and lipid-rich chloroplast (blue) and that from a pixel lying outside the chloroplast but still within the diatom (red) (**Figure 7A** and **B**). False-colour images were obtained by numerical integration of the area under a given biomarker band in each spectrum of the array. Here, the band

intensity for lipid (integrated asymmetric and symmetric CH_2+CH_3 bands lying between 2840 and 2969 cm^{-1}), protein (Amide I centered at 1645 cm^{-1}), and silica (Si-O centered at 1075 cm^{-1}) content illustrate the localized fats and the more generally distributed cellular proteins (**Figure 7C** and **D**, respectively). Cellular saturated lipid and protein content are observed to be greatest in the chloroplast region of the cell (e.g., blue spectrum) versus areas found within the cell but just outside the chloroplast (e.g., red spectrum). Finally, the integrated area of the Si-O band (**Figure 7E**) serves to delineate intact cells.

The images in **Figure 7B–E** display the FTIR hyperspectral image of five intact diatoms, obtained as a 2×2 array. As noted in the Methods section, all images were exported into Matlab™ to provide lipid, protein, and silicate content per diatom pixel, for each diatom in every image (Findlay et al., 2015; Pogorzelec et al., 2017); data are presented in summary form in **Table 1**.

Nitzschia frigida and *Attheya* spp.

The cellular saturated lipid content per pixel for *Nitzschia frigida* increased significantly towards the outside of the tidal strait (site 4) for the 0–2 cm ice section (**Figure 8A**). Vertically, no significant differences in lipid content between ice sections were observed (**Table 1**), though lipid content appeared to increase slightly vertically. The *Attheya* spp. lipid content did not vary horizontally

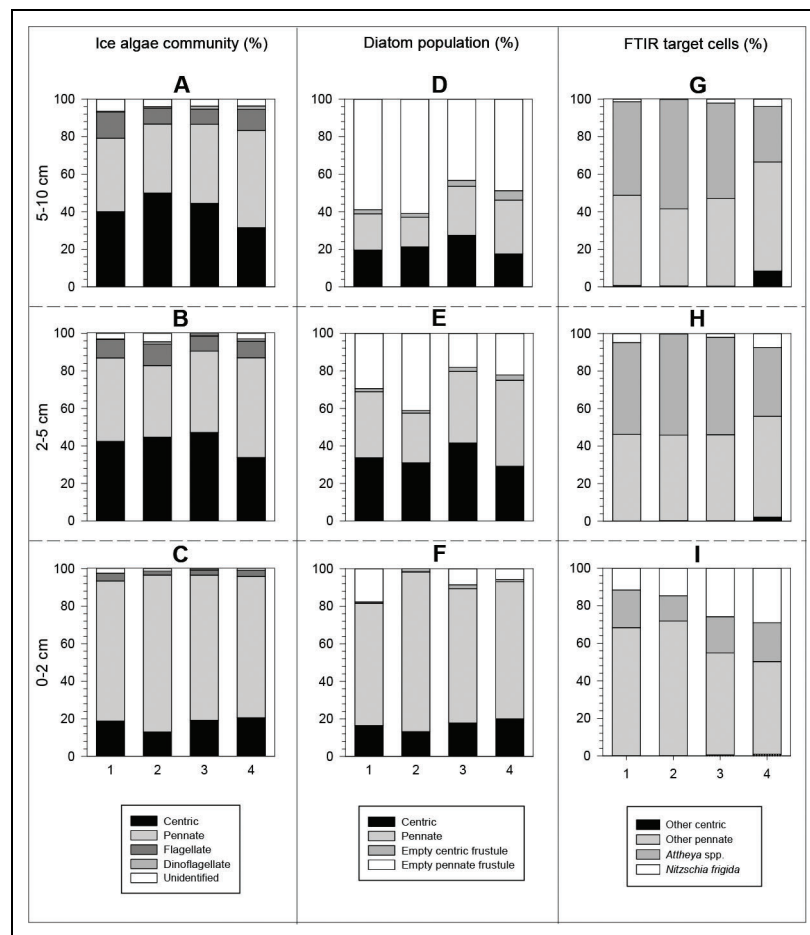


Figure 5. Relative taxonomic compositions of ice algae in bottom sea ice along the horizontal transect. Relative composition of: the ice algal community within ice sections (A) 5–10 cm, (B) 2–5 cm, and (C) 0–2 cm; the diatom population including intact cells and empty frustules within ice sections (D) 5–10 cm, (E) 2–5 cm, and (F) 0–2 cm; and the targeted FTIR diatom contribution to the intact-cell diatom population within ice sections (G) 5–10 cm, (H) 2–5 cm, and (I) 0–2 cm for each of the 4 sites sampled (x-axis).

across the sites in the 0–2 cm layer (**Figure 8B**). However, averaged saturated lipid content differed significantly between ice sections (0–2 versus 2–5 cm; **Table 1**), increasing by an order of magnitude from the 0–2 cm ice section (**Figure 8B**) to the 2–5 and 5–10 cm layers (**Table 1**).

Horizontally, cellular protein content of *Nitzschia frigida* in the 0–2 cm ice section decreased significantly across the entire transect, from sites 1 to 4 (**Figure 8C**). Vertically, averaged protein content of this species did not differ significantly between ice sections (**Table 1**). Cellular protein content of *Attheya* spp. (**Figure 8D**) in the 0–2 cm layer also decreased significantly from sites 1 to 4, but no significant vertical differences in protein content were detected between sections (**Table 1**).

Finally, the lipid:protein ratios were compared for the two taxa. In *Nitzschia frigida*, the ratio increased significantly from site 1 to site 4 (**Figure 8E**) in the 0–2 cm layer. Once again, no vertical difference in ratio values was observed across the sites (**Table 1**). In *Attheya* spp. (**Figure 8F**), the ratio also increased significantly from site 1 to site 4 in the 0–2 cm layer. However, in contrast to *N. frigida*, the ratio values for *Attheya* spp. differed

significantly between most ice sections, nearly doubling between the 0–2 and 5–10 cm layers (**Table 1**).

Discussion

Studies of the ice algal community along a vertical fine-structure gradient (Smith et al., 1990; Gradinger, 1999), across a tidal strait (Dalman et al., 2019), and over fortnightly tidal cycles (Gosselin et al., 1985; Cota et al., 1987) have helped to demonstrate that nutrient supply gradients, via ocean-ice fluxes to the bottom-ice algal community, can greatly influence standing stocks and production of that community. The use of FTIR to analyse minute changes in biomolecular composition of bulk algal cells in natural (Giordano et al., 2001; Stehfest et al., 2005; Dean et al., 2010) and culture-based communities (Heraud et al., 2008; Sackett et al., 2013; Sackett et al., 2016), as well as in individual field sampled diatoms (Findley et al., 2015; Pogorzelec et al., 2017), has been very successful. Here, we examined the biomolecular composition of individual diatom cells, using FTIR spectrochemical imaging, in response to two expected nutrient supply gradients in their natural environment.

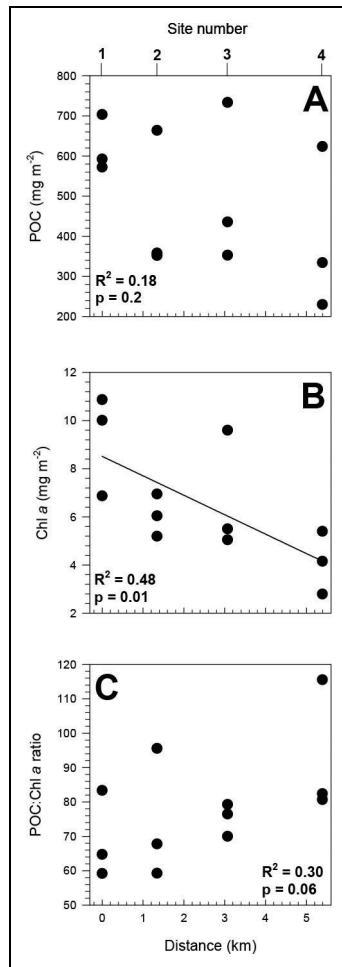


Figure 6. Biomass of the bulk ice algal community in bottommost sea ice along the horizontal transect.

Concentrations of (A) particulate organic carbon (POC) and (B) chlorophyll *a* (Chl *a*; $y = 8.52 - 0.81x$) as proxies for the bulk ice algal community, and ratios of (C) POC:Chl *a* observed in the 0–2 cm sea-ice section across the 4 sample sites. The solid line represents a significant linear trend.

Bottom-ice algal response across the tidal strait: Horizontal variation

Light availability to the bottom-ice algal community is greatly attenuated by the high scattering properties and thickness of the overlying snow and sea-ice cover (Perovich et al., 1998; Perovich, 2018). Despite our best efforts to target a similar snow depth at all sites, snow depth at site 4 was significantly less than at all other sample sites (Figure 3). However, percent PAR transmittance to the ice bottom did not follow a horizontal trend, presumably due to the small snow depth difference (<2 cm), an equal surface albedo and an increase in ice thickness towards site 4 (approximately 170 cm). The lack of a significant change in PAR transmittance supported the assumption of a minimal influence of light variability on algal properties across sites. The lower ice thickness at sites 1 and 2 agreed with previous observations (Dalman et al., 2019) where greater under-ice tidal currents increased ocean-ice heat fluxes, impeding ice growth within the tidal strait. This

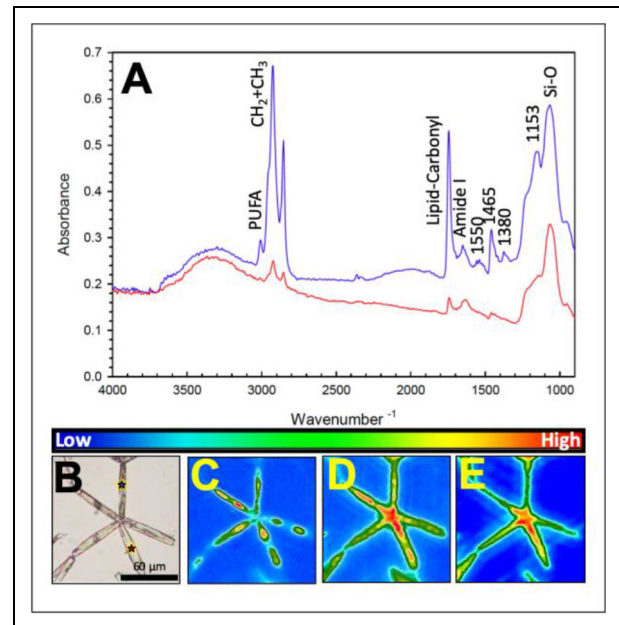


Figure 7. FTIR spectra of *Nitzschia frigida* with false colour images depicting biochemical content. (A) FTIR spectra of a *N. frigida* cell corresponding to red (outside chloroplast) and blue (inside chloroplast) lines, with (B) a light microscopic image of a representative *N. frigida* colony (red and blue stars denote locations of spectra plotted in A) and corresponding false-colour images processed to illustrate integrated band areas for (C) saturated CH₂+CH₃ (lipid), (D) Amide I (protein), and (E) Si-O (silica) across the data array.

process has led these regions to be referred to as invisible polynyas (Melling et al., 2015). Support of a greater ocean-ice heat flux also implies a greater nutrient flux from the underlying water column (Dalman et al., 2019), suggesting that we sampled a horizontally decreasing gradient in nutrient supply from site 1 to 4. Under-ice currents were not measured during our study.

Dease Strait, including the Finlayson Islands through which the tidal strait was sampled, has been reported to be a nitrogen-deplete environment, limiting local ice algal production (Campbell et al., 2016; Kim et al., 2020). This previously determined growth-limiting nutrient averaged 1.5 mmol L⁻¹ nitrate+nitrite, with a mol:mol ratio of 0.27 against silicic acid, indicating nitrogen depletion in the region. This ratio is roughly half of that in the adjacent source Pacific water mass, which tends to have a nitrate:silicic acid molar ratio of 0.5, with nitrate concentrations up to 15 mmol L⁻¹ (Carmack et al., 2004). In-ice nutrient concentrations were observed to be greatest in the 0–2 cm ice section (Figure 4B–D). However, no significant difference was observed horizontally across the four sites. The high variability in bottom-ice salinity and nutrient concentrations observed during the study could be influenced by the length of the study, which spanned a fortnightly tidal cycle. Furthermore, the Arctic ice algal community can exhibit a nutrient concentration mechanism, where dissolved inorganic nutrients vary with bottom-ice algal

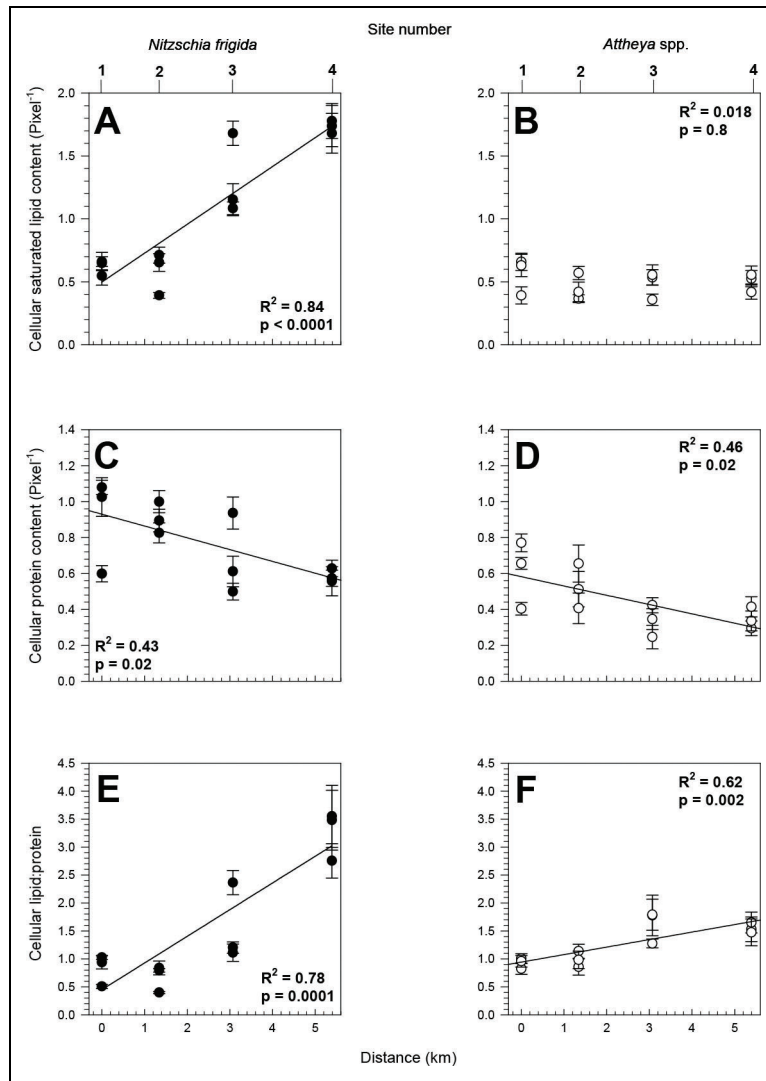


Figure 8. Diatom biomolecular composition from FTIR in bottommost sea ice along the horizontal transect. Sample-averaged FTIR-estimated cellular biomolecular compositions (\pm standard error bars) of (A, C, and E) *Nitzschia frigida* (black symbols) and (B, D, and F) *Attheya* spp. (white symbols) in the 0–2 cm sea-ice layer across the 4 sample sites: (A, B) saturated lipid ($y = 0.50 + 0.23x$); (C, D) protein ($y = 0.95 - 0.07x$ and $y = 0.58 - 0.05x$), and (E, F) saturated lipid:protein ratio ($y = 0.45 + 0.48x$ and $y = 0.94 + 0.13x$). All values are per pixel. Solid lines represent significant linear trends.

biomass (e.g., Cota et al., 1990; Pineault et al., 2013; Dalman et al., 2019). This mechanism explains the greater nutrient concentrations typically observed in a bottom-ice algal community than in the underlying water column (Dalman et al., 2019), which include the relatively high phosphate concentrations and variability observed in our study. However, the mechanism is not well-understood with respect to nutrient availability, though it may be a function of either intracellular uptake and storage by ice algae (Cota et al., 1990) or build-up in the extracellular biofilm of the community (Roukaerts, 2018).

There was also no discernible change in pennate diatom contribution to composition of the bottom-ice community across the tidal strait (Figure 5). This lack of change contrasts with the results from Dalman et al. (2019), who observed a slight decrease in pennate relative abundance away from the tidal strait and hypothesized that the change was a function of decreased ocean-ice

nutrient supply. Furthermore, only Chl *a* concentration in the ice exhibited a significant decrease away from the tidal strait, with no significant trends observed in POC concentration or the POC:Chl *a* g:g ratio (Figure 6). Although there was a weak increasing trend in POC:Chl *a* toward site 4 that could support a pattern of increasing nutrient stress, concluding from these results that a horizontal relationship existed across the tidal strait, as observed by Dalman et al. (2019), would be difficult. Furthermore, these bulk measurements do not provide information regarding specifics of the ice algal community, such as relative condition of algal cells, as they include all sea-ice inhabitants and organic particles.

In contrast to the bulk measurements of POC and Chl *a*, clear horizontal trends were observed in the biomolecular composition of *Nitzschia frigida* and *Attheya* spp. cells across the tidal strait as measured with FTIR. A significant increase in saturated lipid content towards the outside of

the tidal strait was observed in *N. frigida*, but no trend was observed across sites for *Attheya* spp. (Figure 8A and B). The cellular protein content decreased significantly and the lipid:protein ratio increased significantly beyond the tidal strait for both *N. frigida* and *Attheya* spp. (Figure 8C–F).

Photosynthate allocation of carbon within the cell can be altered by light availability or nutrient stress or both (Smith et al., 1997; Mock and Kroon, 2002a; 2002b). During the early portion of the bloom, when nutrient supply is higher relative to the algal standing stock and thus nutrient demand (Gradinger, 2009; Dalman et al., 2019), ice algae divert photosynthesis-assimilated carbon to protein production. When nutrients become limiting, the allocation of carbon is diverted away from protein production and protein-enriched complexes, such as the chloroplast's photosystem II, to lipid production (Smith et al., 1997; Giordano et al., 2001; Mock and Kroon, 2002a; Stehfest et al., 2005). The latter response is also expected to increase with increasing light availability (Mock and Kroon, 2002b). The fact that no significant difference in PAR transmittance was observed across sites in our study decreases the likelihood of mis-identifying biomolecular changes as being a consequence of light availability. The observed changes in biomolecular composition of both *N. frigida* and *Attheya* spp. cells could thus be interpreted as a response to nutrient deficiency within the ice algal community. Therefore, we interpret these results as support for the existence of a greater nutrient supply towards the centre of the tidal strait, as concluded in Dalman et al. (2019). Furthermore, the greater increase in saturated fatty acids in *N. frigida* cells relative to that of *Attheya* spp. cells across the tidal strait supports greater sensitivity to changes in nutrient availability as a function of the larger size and greater nutrient demand of *N. frigida* cells (Pogorzelec et al., 2017).

Ice algal response up into the bottom-ice matrix:

Vertical variation

Nutrient, POC and Chl *a* concentrations all decreased significantly away from the ocean-ice interface (from 0–2 to 5–10 cm). Within the bottom-ice 2–10 cm section, algae were starved of nutrients, with averaged nitrate+nitrite, silicic acid, and phosphate concentrations of 0.4, 1.3, and 0.3 mmol L⁻¹, respectively. The difference vertically between ice sections was accentuated when comparing the POC:Chl *a* g:g ratio, which increased from <100 in the bottom 0–2 cm section to >450 in the 5–10 cm section. Lower values of the POC:Chl *a* ratio can indicate a greater contribution of active photosynthetic cells to the POC pool, with the ratio slightly increasing under greater light availability due to decreased pigment production with light acclimation and greater lipid production (Gosselin et al., 1990; Kirst and Wiencke, 1995; Mock and Kroon, 2002b). However, substantial increases should be associated with nutrient stress such as arises during post-bloom conditions (Mock and Kroon, 2002a). The significant increase in the POC:Chl *a* ratio away from the ocean-ice interface likely indicated a mostly trapped ice algal

community that was in a post-bloom state with depleted nutrient resources.

Higher into the bottom-ice matrix, centric diatoms increased in relative abundance to become the dominant taxa, even though a significant decrease in absolute abundance was observed for all algal cells. Other ice algal taxa (e.g., flagellates and dinoflagellates) also increased in relative contribution as was observed in Gradinger (1999). Dominance by the smaller centric diatom cells has been explained by less stress under nutrient-limiting conditions relative to that of larger pennate cells, such as *Nitzschia frigida* (Pogorzelec et al., 2017; Campbell et al., 2018), or by an increase in light availability (Róžańska et al., 2009). With respect to light availability, assuming a bottom-ice attenuation coefficient of 3.2 m⁻¹ (Ehn and Mundy, 2013), the difference between the ice bottom and 10 cm upwards into the ice matrix would be approximately 0.75% of PAR transmittance. This difference fits within the range of PAR transmittance observed across our sites. However, invoking a slightly greater attenuation coefficient is likely a more reasonable way to account for the bulk ice algal concentration in the bottom 0–10 cm, which equates to 75 mg m⁻³ (Table 1). Using the equation provided in Ehn and Mundy (2013), an attenuation coefficient of 8.7 m⁻¹ is obtained for this Chl *a* concentration, which equates to a change of approximately 2.75% PAR transmittance over the 10-cm ice-bottom section. This vertical change in light availability is slightly greater than the horizontal variability, and thus its potential influence on the algal community cannot be ignored. However, the vertical change in nutrient concentration was much greater than its horizontal variability, again supporting a greater influence of decreasing nutrient availability upwards into the ice bottom (Figure 4B–D, Table 1).

The increase in proportion of empty pennate frustules, but not centric frustules, can suggest a greater stress on the larger pennate cells (Figure 5). However, the biomolecular response also highlights an alternative possibility. Lipid content in *Nitzschia frigida* only increased vertically from the 0–2 to 2–5 cm section (Table 1). In contrast, *Attheya* spp. lipid content significantly increased from the 0–2 cm section to both the 2–5 and 5–10 cm sections. Additionally, only the *Attheya* spp. lipid:protein ratio significantly increased across all ice sections. These results suggest a greater stress on *Attheya* spp. cells higher up in the ice matrix. As discussed above, when nutrients (particularly nitrogen) become limiting, protein production is reduced and a greater allocation of carbon to lipid production occurs (Smith et al., 1997; Mock and Kroon, 2002a; Pogorzelec et al., 2017). We hypothesize that the *Attheya* spp. cells were trapped and cut-off from any nutrient supply, and therefore, a change in protein content would not be expected as cells would not be growing and dividing. However, continued photosynthesis by individual cells could result in increased lipid production, as observed in our results. The vertical change in *Attheya* spp. biomolecular composition and the lesser response of that by *N. frigida* cells are somewhat counterintuitive relative to the taxonomic composition observations which suggested a shift towards centric diatom community

dominance away from the ocean-ice interface. The discrepancy between the relative increase in *N. frigida* empty frustules versus no change for that in *Attheya* spp. could potentially be explained by sample processing. That is, the thin and fragile *Attheya* spp. frustules could have been broken down more easily during sample processing and storage and thus be indiscernible during cell enumeration. Also, epiphytic associations between *Attheya* spp. and much larger pennate cells (Poulin et al., 2011) were only observed in the 0–2 cm ice section. While the host diatom cannot provide a transfer of nutrients to the epiphytic diatom (Cattaneo and Kalff, 1979; Emlinson and Moss, 1980), it may aid in bringing the epiphyte into a more nutrient-rich zone. Therefore, we surmise that a lack of epiphytic host higher in the ice, combined with very limited access to ambient nutrients, greatly influenced metabolic functions of the individual *Attheya* spp. cells (i.e., the lipid:protein ratio).

The lack of vertical change in lipid:protein content of *Nitzschia frigida* could also be due to multiple other factors. Firstly, *N. frigida* can decrease metabolism (Aletsee and Jahnke, 1992; Zhang et al., 1998) and potentially exhibit a heterotrophic strategy, possibly utilizing previously exuded extracellular polymeric substances as a nutrient resource (Niemi et al., 2011). These strategies could minimize changes in biomolecular composition vertically in the ice matrix. Secondly, as a raphid pennate diatom (Medlin and Hasle, 1990), *N. frigida* has the capacity to glide across surfaces (Wetherbee et al., 1998). Indeed, the capacity of sea-ice pennate diatoms to move vertically through the sea-ice matrix in response to changes in light and nutrient access has been demonstrated (Aumack et al., 2014). The potential for vertical motility of *N. frigida* cells could mask the observation of a vertical response in biomass composition of this taxon within the bottom-ice matrix, and the opposite for non-motile centric diatoms (e.g., *Attheya* spp.) that would be trapped in place within the accreting bottom-ice environment.

Additional work is required to fully elucidate the physical and biological processes that led to our observations. However, without the FTIR technique and its corresponding estimates of cellular biomass composition, interpretation of the vertical response in biomass composition of the ice algal community would have been greatly limited. The same is true of the results for horizontal variability, where changes in biomass composition based on FTIR analysis of individual diatoms strongly supported the existence of a nutrient gradient across the Finlayson Islands tidal strait. In stark contrast, drawing meaningful conclusions from the bulk measurements (i.e., POC, Chl *a* and POC:Chl *a* ratio) was not possible. Application of FTIR spectroscopy for autecological research on diatoms is still a relatively new and rarely used technique. Given the usefulness demonstrated here, we strongly encourage application of the technique to future ecological studies of sea-ice diatoms.

Data accessibility statement

All data and metadata are located at <https://canwin-datahub.ad.umanitoba.ca/data/dataset/ftir-taxa> (doi:10.5203/vvtz-x259).

Supplemental files

The supplemental files for this article can be found as follows:

Table S1. Study-averaged (\pm standard deviation) bottom-ice section bulk ice salinity and dissolved inorganic nutrient concentrations and pertinent statistical results comparing differences among sample sites (distance), bottom-ice vertical sections, and sample date. Docx

Acknowledgments

Special thanks are extended to Dr. David Capelle for MATLAB support, Canada High Arctic Research Station (CHARS) operated by Polar Knowledge Canada for logistic support and housing, the Ekaluktutiak Hunters and Trappers Organization, Willie Nakashook, Pamela Nakashook, Tommy Ekpakohak, and Jimmy Haniliak for guiding us, and the community of Cambridge Bay, Nunavut, CA for supporting the research conducted during the 2017 ICE-CAMPS field campaign. This work represents a contribution to the Arctic Science Partnership (ASP) and the Canada Excellence Research Chair (CERC) unit at the University of Manitoba.

Funding

The 2017 ICE-CAMPS project was supported by funding from the Northern Scientific Training Program award to NMP, Natural Science and Engineering Research Council of Canada (NSERC) Discovery Grants to CJM and KMG. and Northern Research Supplement to CJM, and the Kitikmeot Region Marine Science Study, a Polar Knowledge Canada grant to the Arctic Research Foundation (ARF). Additional support was provided by the Marine Environmental Observation Prediction and Response Network (MEOPAR), a Networks of Centres of Excellence (NCE) program. Research support for SHL was provided by Korea Institute of Marine Science & Technology Promotion (KIMST) funded by the Ministry of Oceans and Fisheries (20210605, Korea-Arctic Ocean Warming and Response of Ecosystem, KOPRI). Field and laboratory instruments from the Arctic Biogeochemical Optics Laboratory (ABOL) were originally purchased through Canada Foundation for Innovation- John R. Evans Leaders Fund and Research Manitoba grants to CJM and Dr. Jens K. Ehn. FTIR was purchased with assistance from Western Economic Diversification Canada (Winnipeg Partnership Agreement) and the University of Manitoba Faculties of Science and Engineering.

Competing interests

The authors have no competing interests to declare.

Author contributions

Contributed to conception and design: NMP, KMG, CJM.

Contributed to acquisition of data: NMP, S-YH, KK, KC, CJM.

Contributed analysis and interpretation of data: NMP, KMG, CJM.

Drafted and/or revised the article: Author and all co-authors.

Approved the submitted version for publication: Author and all co-authors.

References

- Aletsee, L, Jahnke, J.** 1992. Growth and productivity of the psychrophilic marine diatoms *Thalassiosira antarctica* Comber and *Nitzschia frigida* Grunow in batch cultures at temperatures below the freezing point of sea water. *Polar Biology* **11**(8): 643–647.
- Arrigo, KR.** 2014. Sea ice ecosystems. *Annual Review of Marine Science* **6**: 439–467. DOI: <http://dx.doi.org/10.1146/annurev-marine-010213-135103>.
- Aumack, CF, Juhl, AR, Krembs, C.** 2014. Diatom vertical migration within land-fast Arctic sea ice. *Journal of Marine Systems* **139**: 496–504.
- Campbell, K, Mundy, CJ, Barber, DG, Gosselin, M.** 2015. Characterizing the sea ice algae chlorophyll *a*-snow depth relationship over Arctic spring ice melt using transmitted irradiance. *Journal of Marine Systems* **147**: 76–84.
- Campbell, K, Mundy, CJ, Belzile, C, Delaforge, A, Rysgaard, S.** 2018. Seasonal dynamics of algal and bacterial communities in Arctic sea ice under variable snow cover. *Polar Biology* **41**: 41–58.
- Campbell, K, Mundy, CJ, Gosselin, M, Landy, J, Delaforge, A, Rysgaard, S.** 2017. Net community production in the bottom of Arctic sea ice over the spring bloom. *Geophysical Research Letters* **44**: 8971–8978. DOI: <http://dx.doi.org/10.1002/2017GL074602>.
- Campbell, K, Mundy, CJ, Juhl, A, Dalman, LA, Michel, C, Galley, R, Else, BE, Geilfus, NX, Rysgaard, S.** 2019. Melt procedure affects the photosynthetic response of sea ice algae. *Frontiers in Earth Science* **7**(21): 14. DOI: <http://dx.doi.org/10.3389/feart.2019.00021>.
- Campbell, K, Mundy, CJ, Landry, JC, Delaforge, A, Michel, C, Rysgaard, S.** 2016. Community dynamics of bottom-ice algae in Dease Strait of the Canadian Arctic. *Progress in Oceanography* **149**: 27–39.
- Carmack, EC, Macdonald, RW, Jasper, S.** 2004. Phytoplankton productivity on the Canadian Shelf of the Beaufort Sea. *Marine Ecology Progress Series* **277**: 37–50.
- Cattaneo, A, Kalff, I.** 1979. Primary production of algae growing on natural and artificial aquatic plants. A study of interactions between epiphytes and their substrate. *Limnology and Oceanography* **24**: 1031–1037.
- Comiso, JC, Parkinson, CL, Gersten, R, Stock, L.** 2008. Accelerated decline in the Arctic sea ice cover. *Geophysical Research Letters* **35**: L01703. DOI: <http://dx.doi.org/10.1029/2007GL031972>.
- Cota, GF, Anning, JL, Harris, LR, Harrison, WG, Smith, REH.** 1990. Impact of ice algae on inorganic nutrients in seawater and sea ice in Barrow Strait, NWT, Canada, during spring. *Canadian Journal of Fisheries and Aquatic Sciences* **47**: 1402–1415.
- Cota, GF, Prinsenberg, SJ, Bennett, EB, Loder, JW, Lewis, MR, Anning, JL, Watson, NHF, Harris, LR.** 1987. Nutrient fluxes during extended blooms of Arctic ice algae. *Journal of Geophysical Research-Oceans* **92**(C2): 1951–1962.
- Cutter, C, Andersson, P, Codispoti, L, Croot, P, Francois, R, Lohan, MC, Obata, H, Rutgers van der Loeff, M.** 2014. Sampling and sample-handling protocols for GEOTRACES cruises, v. 2.0. *GEOTRACES*: 123–125.
- Dalman, LA, Else, BE, Barber, D, Carmack, E, Williams, WJ, Campbell, K, Duke, PJ, Kirillov, S, Mundy, CJ.** 2019. Enhanced bottom-ice algal biomass across a tidal strait gradient in the Kitikmeot Sea of the Canadian Arctic. *Elementa: Science of the Anthropocene* **7**: 22. DOI: <http://dx.doi.org/10.1525/elementa.361>.
- Dean, AP, Sigee, DC, Estrada, B, Pittman, JK.** 2010. Using FTIR spectroscopy for rapid determination of lipid accumulation in response to nitrogen limitation in freshwater microalgae. *Bioresource Technology* **101**: 4499–4507. DOI: <http://dx.doi.org/10.1016/j.biortech.2010.01.065>.
- Ehn, JK, Mundy, CJ.** 2013. Assessment of light absorption within highly scattering bottom sea ice from under-ice light measurements: Implications for Arctic ice algae primary production. *Limnology and Oceanography* **58**: 893–902.
- Eminson, D, Moss, B.** 1980. The composition and ecology of periphyton communities in freshwaters: 1 The influence of host type and external environment on community composition. *British Phycology Journal* **15**: 429–446.
- Findlay, CR, Wiens, R, Rak, M, Sedlmair, J, Hirschmugl, CJ, Morrison, J, Mundy, CJ, Kansiz, M, Gough, KM.** 2015. Rapid biodiagnostic ex-vivo imaging at 1 μ m pixel resolution with thermal source FTIR FPA. *Analyst* **140**: 2493–2503. DOI: <http://dx.doi.org/10.1039/C4AN01982B>.
- Garrison, DL, Buck, KR.** 1986. Organism losses during ice melting: A serious bias in sea ice communities studies. *Polar Biology* **6**: 237–239.
- Giordano, M, Kansiz, M, Heraud, P, Beardall, J, Wood, B, McNaughton, D.** 2001. Fourier transform infrared spectroscopy as a novel tool to investigate changes in intracellular macromolecular pools in the marine microalga *Chaetoceros muellerii* (Bacillariophyceae). *Journal of Phycology* **37**: 271–279. DOI: <http://dx.doi.org/10.1046/j.1529-8817.2001.037002271.x>.
- Gosselin, M, Legendre, L, Demers, S, Ingram, RG.** 1985. Responses of sea-ice microalgae to climatic and fortnightly tidal energy inputs (Manitounuk Sound, Hudson Bay). *Canadian Journal of Fisheries and Aquatic Sciences* **42**: 999–1006.
- Gosselin, M, Legendre, L, Therriault, JC, Demers, S.** 1990. Light and nutrient limitation of sea-ice microalgae (Hudson Bay, Canadian Arctic). *Journal of Phycology* **26**: 220–232.
- Gradinger, R.** 1999. Vertical fine structure of the biomass and composition of algal communities in Arctic pack ice. *Marine Biology* **133**: 745–754.
- Gradinger, R.** 2009. Sea-ice algae: Major contributors to primary production and algal biomass in the Chukchi and Beaufort Seas during May/June 2002. *Deep*

- Sea Research Part II: Topical Studies in Oceanography* **56**: 1201–1212. DOI: <http://dx.doi.org/10.1016/j.dsr2.2008.10.016>.
- Grasshoff, K, Kremling, K, Ehrhardt, M.** 1999. *Methods of seawater analysis*. 3rd ed. New York, NY: Wiley-VCH.
- Griffiths, P, de Haseth, J.** 2007. *Fourier transform infrared spectrometry*. 2nd ed. Hoboken, NJ: Wiley InterScience.
- Heraud, P, Stojkovic, S, Beardall, J, McNaughton, D, Wood, BR.** 2008. Intercolonial variability in macromolecular composition in P-starved and P-replete *Scenedesmus* populations revealed by infrared microspectroscopy. *Journal of Phycology* **44**: 1335–1339.
- Herzberg, G.** 1945. *Infrared and Raman spectra*. New York, NY: Van Nostrand Reinhold Co.
- Hollas, JM.** 2004. *Modern spectroscopy*. 4th ed. Hoboken, NJ: J. Wiley & Sons, Ltd.
- Holm-Hansen, O, Lorenzen, CJ, Holmes, RW, Strickland, JDH.** 1965. Fluorometric determination of chlorophyll. *ICES Journal of Marine Science* **30**: 3–15. DOI: <http://dx.doi.org/10.1093/icesjms/30.1.3>.
- Horner, R, Ackley, SF, Dieckmann, GS, Gulliksen, B, Hoshiai, T, Legendre, L, Melnikov, IA, Reeburgh, WS, Spindler, M, Sullivan, CW.** 1992. Ecology of sea ice biota: 1. Habitat, terminology, and methodology. *Polar Biology* **12**: 417–427.
- Kim, K, Ha, S-Y, Kim, BK, Mundy, CJ, Gough, KM, Pogorzelec, NM, Lee, SH.** 2020. Carbon and nitrogen uptake rates and macromolecular compositions of bottom-ice algae and phytoplankton at Cambridge Bay in Dease Strait, Canada. *Annals of Glaciology* **61**: 106–116. DOI: <http://dx.doi.org/10.1017/aog.2020.17>.
- Kirst, GO, Wiencke, C.** 1995. Ecophysiology of polar algae. *Journal of Phycology* **31**: 181–199.
- Leu, E, Mundy, CJ, Assmy, P, Campbell, K, Gabrielsen, TM, Gosselin, M, Juul-Pedersen, T, Gradinger, R.** 2015. Arctic spring awakening—Steering principles behind the phenology of vernal ice algae blooms. *Progress in Oceanography* **139**: 151–170. DOI: <http://dx.doi.org/10.1016/j.pocean.2015.07.012>.
- Leu, E, Wiktor, J, Søreide, JE, Berge, J, Falk-Petersen, S.** 2010. Increased irradiance reduces food quality of sea ice algae. *Marine Ecology Progress Series* **411**: 49–60. DOI: <http://dx.doi.org/10.3354/meps08647>.
- Lund, JWG, Kipling, C, Le Cren, ED.** 1958. The inverted microscope method of estimating algal number and the statistical basis of estimations by counting. *Hydrobiologia* **11**: 143–170. DOI: <http://dx.doi.org/10.1007/BF00007865>.
- Markus, T, Stroeve, JC, Miller, J.** 2009. Recent changes in Arctic sea ice melt onset, freezeup, and melt season length. *Journal of Geophysical Research: Oceans* **114**: C12024 DOI: <http://dx.doi.org/10.1029/2009JC005436>.
- Medlin, LK, Hasle, GR.** 1990. Some *Nitzschia* and related diatom species from fast ice samples in the Arctic and Antarctic. *Polar Biology* **10**: 451–479.
- Melling, H, Haas, C, Brossier, E.** 2015. Invisible polynyas: Modulation of fast ice thickness by ocean heat flux on the Canadian polar shelf. *Journal of Geophysical Research: Oceans* **120**: 777–795. DOI: <http://dx.doi.org/10.1002/2014JC010404>.
- Michel, C, Ingram, RG, Harris, LR.** 2006. Variability in oceanographic and ecological processes in the Canadian Arctic Archipelago. *Progress in Oceanography* **71**: 379–401. DOI: <http://dx.doi.org/10.1016/j.pocean.2006.09.006>.
- Mock, T, Gradinger, R.** 2000. Changes in photosynthetic carbon allocation in algal assemblages of Arctic sea ice with decreasing nutrient concentration and irradiance. *Marine Ecology Progress Series* **202**: 1–11.
- Mock, T, Kroon, BMA.** 2002a. Photosynthetic energy conversion under extreme conditions-I: Important role of lipids as structural modulators and energy sink under *N*-limited growth in Antarctic sea ice diatoms. *Phytochemistry* **61**: 41–51. DOI: [http://dx.doi.org/10.1016/S0031-9422\(02\)00216-9](http://dx.doi.org/10.1016/S0031-9422(02)00216-9).
- Mock, T, Kroon, BMA.** 2002b. Photosynthetic energy conversion under extreme conditions—II: The significant of lipids under light limited growth in Antarctic sea ice diatoms. *Phytochemistry* **61**: 53–60. DOI: [http://dx.doi.org/10.1016/S0031-9422\(02\)00215-7](http://dx.doi.org/10.1016/S0031-9422(02)00215-7).
- Mock, T, Thomas, DN.** 2005. Recent advances in sea-ice microbiology. *Environmental Microbiology* **7**: 605–619. DOI: <http://dx.doi.org/10.1111/j.1462-2920.2005.00781.x>.
- Niemi, A, Michel, C, Hille, K, Poulin, M.** 2011. Protist assemblages in winter sea ice: Setting the stage for the spring ice algal bloom. *Polar Biology* **34**: 1803–1817.
- Parsons, TR, Maita, Y, Lalli, CM.** 1984. *A manual of chemical and biological methods for seawater analysis*. Elmsford, NY: Pergamon Press.
- Perovich, DK.** 2018. Sunlight, clouds, sea ice, albedo, and the radiative budget: The umbrella versus the blanket. *The Cryosphere* **12**: 2159–2165. DOI: <http://dx.doi.org/10.5194/tc-12-2159-2018>.
- Perovich, DK, Roesler, CS, Pegau, WS.** 1998. Variability in Arctic sea ice optical properties. *Journal of Geophysical Research: Oceans* **103**: 1193–1208.
- Pineault, S, Tremblay, J-E, Gosselin, M, Thomas, H, Shadwick, E.** 2013. The isotopic signature of particulate organic C and N in bottom ice: Key influencing factors and applications for tracing the fate of ice-algae in the Arctic Ocean. *Journal of Geophysical Research: Oceans* **118**: 287–300. DOI: <http://dx.doi.org/10.1029/2012JC008331>.
- Pogorzelec, NM, Mundy, CJ, Findlay, CR, Campbell, K, Diaz, A, Ehn, JK, Rysgaard, S, Gough, KM.** 2017. FTIR imaging analysis of cell content in sea-ice diatom taxa during a spring bloom in the lower Northwest Passage of the Canadian Arctic. *Marine Ecology Progress Series* **69**: 77–88. DOI: <http://dx.doi.org/10.3354/meps12088>.
- Poulin, M, Daugbjerg, N, Gradinger, R, Ilyash, L, Ratkova, T, von Qillfeldt, C.** 2011. The pan-Arctic biodiversity of marine pelagic and sea-ice unicellular

- eukaryotes: A first-attempt assessment. *Marine Biodiversity* **41**: 13–28.
- Rintala, JM, Piiparinen, J, Blomster, J, Majaneva, M, Müller, S, Uusikivi, J, Autio, R.** 2014. Fast direct melting of brackish sea-ice samples results in biologically more accurate results than slow buffered melting. *Polar Biology* **37**: 1811–1822. DOI: <http://dx.doi.org/10.1007/s00300-014-1563-1>.
- Roukaerts, A.** 2018. Novel insights in nitrogen and carbon biogeochemistry of Antarctic sea ice: The potential role of a microbial biofilm [Doctoral dissertation]. Brussels, Belgium: Vrije Universiteit Brussel.
- Rózańska, M, Gosselin, M, Poulin, M, Wiktor, JM, Michel, C.** 2009. Influence of environmental factors on the development of bloom ice protist communities during the winter–spring transition. *Marine Ecology Progress Series* **386**: 43–59. DOI: <http://dx.doi.org/10.3354/meps08092>.
- Sackett, O, Petrou, K, Reedy, B, De Grazia, A, Hill, R, Doblin, M, Beardall, J, Ralph, P, Heraud P.** 2013. Phenotypic plasticity of Southern Ocean diatoms: Key to success in the sea ice habitat? *PLoS One* **8**: e81185. DOI: <http://dx.doi.org/10.1371/journal.pone.0081185>.
- Sackett, O, Petrou, K, Reedy, B, Hill, R, Doblin, M, Beardall, J, Ralph, P, Heraud P.** 2016. Snapshot prediction of carbon productivity, carbon and protein content in Southern Ocean diatom using FTIR spectroscopy. *The ISME Journal* **10**: 416–426.
- Sattar, A, deMan, JM, Alexander, JC.** 1976. Effect of wavelength on light induced quality of deterioration of edible oils and fats. *Canadian Institute of Food Science and Technology Journal* **9**: 108–113.
- Smith, REH, Clement, P, Cota, GF, Li, WK.** 1987. Intracellular photosynthate allocation and the control of Arctic marine ice algal production. *Journal of Phycology* **23**: 124–132.
- Smith, REH, Gosselin, M, Taguchi, S.** 1997. The influence of major inorganic nutrients on the growth and physiology of high Arctic ice algae. *Journal of Marine Systems* **11**: 63–70.
- Smith, REH, Harrison, WG, Harris, LR, Herman, AW.** 1990. Vertical fine structure of particulate matter and nutrients in sea ice of the high Arctic. *Canadian Journal of Fisheries and Aquatic Sciences* **47**: 1348–1355.
- Søreide, JE, Leu, E, Berge, J, Graeve, M, Falk-Petersen, S.** 2010. Timing of blooms, algal food quality and *Calanus glacialis* reproduction and growth in a changing Arctic. *Global Change Biology* **16**: 3154–3163. DOI: <http://dx.doi.org/10.1111/j.1365-2486.2010.02175.x>.
- Stehfest, K, Toepel, J, Wilhelm, C.** 2005. The application of micro-FTIR spectroscopy to analyze nutrient stress-related changes in biomass composition of phytoplankton algae. *Plant Physiology and Biochemistry* **43**: 717–726. DOI: <http://dx.doi.org/10.1016/j.plaphy.2005.07.001>.
- Stitt, DM, Kastyak-Ibrahim, MZ, Liao, CR, Morrison, J, Albensi, BC, Gough, KM.** 2012. Tissue acquisition and storage associated oxidation considerations for FTIR microspectroscopic imaging of polyunsaturated fatty acids. *Vibrational Spectroscopy* **60**: 16–22.
- Stroeve, JC, Serreze, MC, Holland, MM, Kay, JE, Malanik, J, Barrett, AP.** 2012. The Arctic's rapidly shrinking sea ice cover: A research synthesis. *Climatic Change* **110**: 1005–1027. DOI: <http://dx.doi.org/10.1007/s10584-011-0101-1>.
- Tedesco, L, Vichi, M, Scoccimarro, E.** 2019. Sea-ice algal phenology in a warmer Arctic. *Science Advances* **5**: 4830. DOI: <http://dx.doi.org/10.1126/sciadv.aav4830>.
- Vancoppenolle, M, Meiners, KM, Michel, C, Bopp, L, Brabant, F, Carnat, G, Belille, B, Lannuzel, D, Madec, G, Moreau, S, Tison, JL, van der Merwe, P.** 2013. Role of sea ice in global biogeochemical cycles: Emerging views and challenges. *Quaternary Science Reviews* **79**: 207–230. DOI: <http://dx.doi.org/10.1016/j.quascirev.2013.04.011>.
- van Leeuwe, MA, Tedesco, L, Arrigo, KR, Assmy, P, Campbell, K, Meiners, KM, Rintala, J-M, Selz, V, Thomas, DN, Stefels, J.** 2018. Microalgal community structure and primary production in Arctic and Antarctic sea ice: A synthesis. *Elementa: Science of the Anthropocene* **6**: 4. DOI: <http://dx.doi.org/10.1525/elementa.267>.
- Wetherbee, R, Lind, JL, Burke, J, Quatran, RS.** 1998. The first kiss: Establishment and control of initial adhesion by raphid diatoms. *Journal of Phycology* **34**: 9–15.
- Zhang, Q, Gradinger, R, Spindler, M.** 1998. Dark survival of marine microalgae in the high Arctic (Greenland Sea). *Polarforschung* **65**: 111–116.

How to cite this article: Pogorzelec, NM, Gough, KM, Ha, S-Y, Campbell, K, Else, B, Kim, K, Lee, SH, Mundy, CJ. 2022. FTIR autecological analysis of bottom-ice diatom taxa across a tidal strait in the Canadian Arctic. *Elementa: Science of the Anthropocene* 10(1). DOI: <https://doi.org/10.1525/elementa.2021.00094>

Domain Editor-in-Chief: Jody W. Deming, University of Washington, Seattle, WA, USA

Associate Editor: Jean-Éric Tremblay, Department of Biology, Université Laval, Québec, Canada

Knowledge Domain: Ocean Science

Published: December 23, 2022 **Accepted:** November 17, 2022 **Submitted:** October 14, 2021

Copyright: © 2022 The Author(s). This is an open-access article distributed under the terms of the Creative Commons Attribution 4.0 International License (CC-BY 4.0), which permits unrestricted use, distribution, and reproduction in any medium, provided the original author and source are credited. See <http://creativecommons.org/licenses/by/4.0/>.



Elem Sci Anth is a peer-reviewed open access journal published by University of California Press.

OPEN ACCESS The Open Access icon, which is a stylized 'O' with a circular arrow inside, indicating that the content is freely available.